npj Computational Materials

www.nature.com/npjcompumats

ARTICLE OPEN

Mechanistic insights of enhanced spin polaron conduction in CuO through atomic doping

Tyler J. Smart[1], Allison C. Cardiel[2], Feng Wu[3], Kyoung-Shin Choi[2] and Yuan Ping[3]

The formation of a "spin polaron" stems from strong spin-charge-lattice interactions in magnetic oxides, which leads to a localization of carriers accompanied by local magnetic polarization and lattice distortion. For example, cupric oxide (CuO), which is a promising photocathode material and shares important similarities with high T_c superconductors, conducts holes through spin polaron hopping with flipped spins at Cu atoms where a spin polaron has formed. The formation of these spin polarons results in an activated hopping conduction process where the carriers must not only overcome strong electron−phonon coupling but also strong magnetic coupling. Collectively, these effects cause low carrier conduction in CuO and hinder its applications. To overcome this fundamental limitation, we demonstrate from first-principles calculations how doping can improve hopping conduction through simultaneous improvement of hole concentration and hopping mobility in magnetic oxides such as CuO. Specifically, using Li doping as an example, we show that Li has a low ionization energy that improves hole concentration, and lowers the hopping barrier through both the electron−phonon and magnetic couplings' reduction that improves hopping mobility. Finally, this improved conduction predicted by theory is validated through the synthesis of Li-doped CuO electrodes which show enhanced photocurrent compared to pristine CuO electrodes. We conclude that doping with nonmagnetic shallow impurities is an effective strategy to improve hopping conductivities in magnetic oxides.

npj Computational Materials (2018)4:61 ; doi:10.1038/s41524-018-0118-3

INTRODUCTION

In general, transition metal oxide (TMO)-based photoelectrodes used for photoelectrochemical cells (PECs) suffer from low carrier conductivity, which fundamentally limits TMO-based photoelectrodes from reaching higher theoretical photon-to-current efficiencies.[1,2] Although many experimental studies have shown that appropriate doping can effectively boost the photocurrent generation of TMO-based photoelectrodes, attempts to understand the exact effect of the dopants have been very limited, making it difficult to methodically conduct future studies on the optimization of TMO-based photoelectrodes.[3,4]

In this work, we investigated hole transport in cupric oxide (CuO), a p-type semiconductor. Due to its relatively small bandgap (1.2–1.8 eV) and a conduction band minimum located at a more negative potential than that of water reduction,[5–14] it has the potential to serve as an inexpensive and environmentally benign photocathode for a water splitting PEC. However, like other TMOs, CuO suffers from poor carrier conductivity, which limits the effectiveness of CuO-based devices.[12,13,15,16] Additionally, cathodic photocorrosion of CuO can also limit the use of CuO for photoelectrochemical applications. Fortunately, a recent study demonstrated that the photocorrosion of CuO can be effectively suppressed by depositing a thin protection layer that prevents direct contact of CuO and the electrolyte,[14] which encourages studies on further improving charge transport and photoelectrochemical properties of CuO. Facilitated charge transport in CuO can also be advantageous for the use of CuO in other electrochemical devices such as gas sensors.[17,18]

The development of charge transport in CuO depends on the understanding and optimization of the small polaron hopping process. Strong electron−phonon coupling in many TMOs (Fe_2O_3, $BiVO_4$, TiO_2) leads to the localization of carriers into polarons, a quasi-particle representing the carrier and local lattice distortion.[2,19,20] Due to this localization, carriers are no longer transported through the system via typical band mechanisms. Rather, carriers must be thermally activated in order to "hop" between sites, a process known as polaron hopping conduction.[21,22] This type of conduction leads to an extremely low carrier mobility (e.g. 0.1 cm^2/Vs for CuO),[2] several orders of magnitude lower than band-like semiconductors such as Si (~1000 cm^2/Vs). Previous experimental studies have indicated that polaron formation also occurs in CuO.[23–27] Interestingly, more exotic properties such as "one-dimensional charge stripes" and "spin polarons" have been found in CuO due to strong spin-charge-lattice interactions,[25] which distinguishes its conduction mechanism from the common electron polaron hopping conduction in nonmagnetic oxides such as $BiVO_4$. However, there has yet to be a theoretical investigation on the existence and transport of polarons in CuO, which would provide deeper understanding of carrier transport and therefore offer effective doping strategies to improve the carrier transport properties in CuO and other magnetic oxides in general. Finally, although there have been a few experimental doping studies of CuO to date,[16,27–34] the role of

[1]Department of Physics, University of California, Santa Cruz, CA 95064, USA; [2]Department of Chemistry, University of Wisconsin, Madison, WI 53706, USA and [3]Department of Chemistry and Biochemistry, University of California, Santa Cruz, CA 95064, USA
Correspondence: K-S. Choi (kschoi@chem.wisc.edu) or Yuan Ping (yuanping@ucsc.edu)
These authors contributed equally: Tyler J. Smart, Allison C. Cardiel.

Received: 28 May 2018 Accepted: 22 October 2018
Published online: 19 November 2018

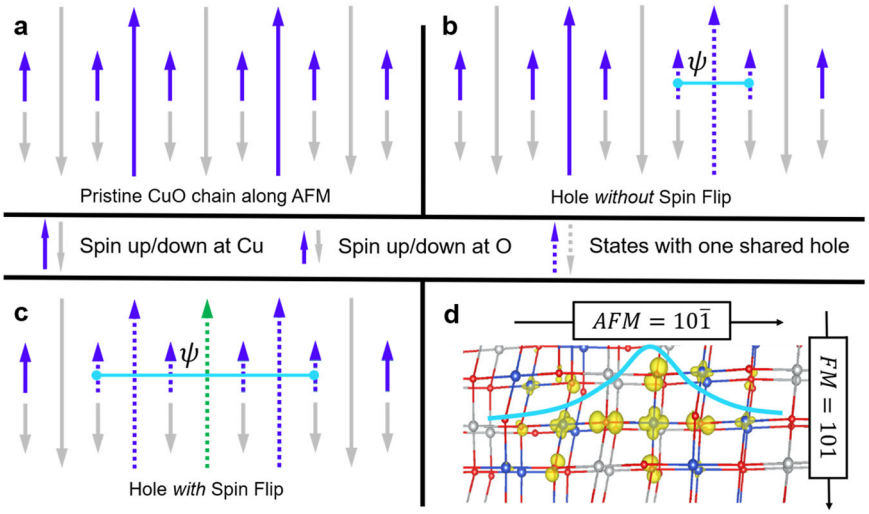

Fig. 1 Spin polaron formation in CuO. **a** Pristine Cu and O chain with antiferromagnetic (AFM) ordering. **b** If a hole forms (without a spin-flip) it will be highly localized as it can only distribute on one Cu atom (other neighboring Cu atoms do not have an available state of the appropriate spin as explained in the main text). **c** After a Cu's moment flips, the hole can redistribute over several Cu atoms lowering the kinetic energy. **d** The wavefunction of a hole in CuO which has formed an SP with a flipped Cu spin so that it may redistribute over several atoms, in accordance with panel (**c**). An isosurface of 10% of the maximum is used (blue ball = Cu with up spin, gray ball = Cu with down spin, and red ball = O). (In panels **a**–**c** large arrows denote the unpaired spin of Cu, small arrows denote two spin states of O which are often paired, dashed arrows denote states with a shared hole, blue/gray arrows = up/down, and green arrow = flipped Cu spin.)

dopants in improving hole conduction in CuO has not been clearly understood.

In this study, we address these fundamental questions by comparatively investigating hole conduction in pristine and Li-doped CuO. Our focus is on the elucidation of the mechanisms by which Li doping improves hole concentration and mobility through a combined theoretical and experimental effort. Our work is organized as follows. First, we provide theoretical background on CuO and discuss the mechanism of hole conduction that involves a unique spin-flip hopping process of spin polarons. Second, we show how Li doping enhances hole concentrations and hole mobility in CuO. Finally, we confirm our theoretical results by preparing CuO and Li-doped CuO electrodes and experimentally comparing their photoelectrochemical properties.

RESULTS AND DISCUSSION

Polaron formation and hole conduction in CuO from first-principles

Several experimental studies have shown that CuO has an Arrhenius dependence of conductivity to temperature.[23–27] This dependence is expected for materials which form small polarons (a trapped electron or hole due to local lattice distortion) which must be thermally activated in order to hop between lattice sites in the material, a process known as polaron hopping.[22] The mobility of small polaron hopping follows the relationship shown in Eq. 1,

$$\mu \propto e^{-E_a/kT}, \quad (1)$$

where E_a is the activation energy, k is the Boltzmann constant, T is the temperature, and μ is the carrier mobility which is related to the conductivity σ, by $\sigma = en\mu$ (n is majority carrier concentration, which are holes in this case). To confirm the presence of polarons in CuO, we computed the electronic structure of pristine CuO with a single electron removed from a 96 atom system ($2 \times 3 \times 2$ supercell), corresponding to a hole concentration of 2% (at. % of hole = 100 × [mol of hole] / [mol of O]). Detailed descriptions of our electronic structure calculations can be found below under the Computational Methods section and SI. From the density of states and wavefunction of the hole state, we determine that holes form localized polaron states. These polaron states are predominantly O *2p* mixed with Cu *3d* as seen from the partial density of states (Figure S2) in agreement with previous studies on the electronic structure of CuO.[35]

An intriguing consequence of hole localization around a single Cu $3d^9$ ion is that the Cu magnetic moment will flip, forming a "spin polaron" (SP).[36–41] Such states are common in copper oxides as the combination of two SPs will create a spinless Cooper pair state which obeys Bose–Einstein statistics and is the basis of superconducting.[38,42] In general, an SP forms in polaronic materials where the kinetic energy of the state can be lowered substantially from the increased delocalization of the electron or hole wavefunction after the spin-flip occurs.[43] For example, after an electron at a spin-up state is removed, a hole is created at the same spin state. As a fermion, the hole obeys the Pauli exclusion principle like electrons and can only be added to a state which is already occupied (i.e. a state must be occupied by an electron of the same spin for a hole to form). Therefore, in an antiferromagnetic system, the delocalization of a spin-up hole is limited by the availability of neighboring atoms' spin-up occupied states. As shown in Fig. 1b, with antiferromagnetic ordering, the hole polaron may form into a highly localized state (limited to forming over a single Cu atom and its bonding O atoms that have up spins, as neighboring Cu atoms do not have an available spin-up state at which the hole can form). But after a neighboring Cu ion's moment flips (Fig. 1c) an extra channel is created, and the spin-up hole can redistribute over several sites that all have an up spin, lowering the kinetic energy of the hole polaron. The resulting flipped Cu ion with a distributed polaron state over several Cu and O atoms is shown in Fig. 1d. As discussed in ref. [43] this lowering of kinetic energy through wavefunction delocalization dominates over the energy cost of the spin-flip and facilitates the formation of spin polarons in CuO. Additional explanations can be found in the SI (Figures S3-S4).

Considering that the magnetic couplings between Cu ions in CuO are significantly large ($J \sim 100$ meV), spin-spin interactions will have an important effect on the conduction of holes in CuO. To address this point, we consider the total kinetic rate κ of the

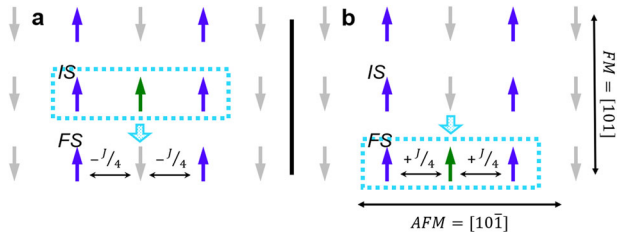

Fig. 2 Spin polaron hopping in pristine CuO. Diagram describing the interplay of spin and polaron hopping in CuO. As opposed to Fig. 1, only Cu spins are shown here for simplicity. **a** Initially the spin polaron has formed at the initial site (*IS*), while the moment of Cu ions at the final site (*FS*) are aligned antiferromagnetically (AFM) (–*j*/4). **b** After the polaron hops to the final site (*FS*) the center Cu moment is flipped, costing energy according to the strength of *J* (blue = Cu with up spin, gray = Cu with down spin, green = Cu with flipped spin, dashed light blue box = polaron state)

hopping process in Eq. 2,

$$\kappa = \frac{\sum_i e^{-E_i/kT}\kappa_i}{\sum_i e^{-E_i/kT}}, \tag{2}$$

where E_i is the energy of the *i*th configuration and κ_i is the hopping rate between configurations (for full details, see SI). For the case of CuO, we found that the formation of a polaron at a site without a flipped spin was not possible, and, presumably, the total energy of such a state is very high, which reduces the possible configurations entering Eq. 2. Then we define hopping that does not involve a spin-flip process to have a rate given by $\kappa_i = e^{-E_a^{e-ph}/kT}$, with E_a^{e-ph} being the usual hopping activation energy barrier due to electron−phonon interactions. We have shown that the Boltzmann factors that are related to the energies of different spin configurations will be dominated by the most probable hopping path (Figure S9). As a result, the full hopping rate κ then reduces to Eq. 3,

$$\kappa \sim e^{-\left(E_a^{e-ph}+E_a^{spin}\right)/kT}. \tag{3}$$

Namely as holes are conducted through the system they will invoke a spin-flip process which will cost energy equal to the cost of flipping a spin of a Cu ion (illustrated in Fig. 2). In final, we see that the energy of this spin-flip process E_a^{spin} can be simply added to the electron−phonon process E_a^{e-ph} to give the full activation energy E_a, given in Eq. 4.

$$E_a = E_a^{e-ph} + E_a^{spin}. \tag{4}$$

Intuitively, a spin-flip hopping process will not have a well-defined transition state; if there was a transition state, it would be a spin delocalized state which is not favored to form in a polaronic oxide. To confirm this point, we employed the newly developed constrained density functional theory technique for solids in which an external potential is added to the Kohn−Sham potentials, and its strength is varied self-consistently in order to localize a desired number of charges on a specific site.[44,45] This allows for a direct calculation of the electronic coupling constant between initial and final states $|H_{ab}|$ in CuO, which we obtained to be 1.01 meV (the numerical accuracy is 0.01 meV). This is two orders of magnitude smaller than the computed activation energy (shown later), implying that transport in CuO is indeed non-adiabatic, which cannot be described by a semi-classical transition state theory.

The energy of this spin-flip (E_a^{spin}) can be obtained directly using the Heisenberg Hamiltonian $H_{spin} = -\sum_{i<j} J_{ij}\widehat{S}_i \cdot \widehat{S}_j$, where J_{ij} is the magnetic coupling between the spin of the *i*th and *j*th Cu ion and $\widehat{S}_i$ is the spin of the *i*th Cu ion (taken to be ½ as Cu is in a $3d^9$ configuration with one unpaired electron). The use of this model is well-established in accurate modeling of the magnetic couplings of CuO,[46–48] and our calculations show that fitting the total energy of different magnetic configurations of CuO with this Hamiltonian yields an *R*-squared of 0.999 (Figure S7). Following a previous work,[46] we considered five magnetic couplings in CuO: J_z, J_x, J_a, J_b, J_2. Of these five couplings, the coupling J_z is dominant over the rest with a value of −111 meV and is responsible for the long-range antiferromagnetic transition of CuO at 230 K. Note that in CuO the magnetic correlation length remains large at temperatures above the transition temperature T_N, so magnetic coupling is still relevant to our discussion of hole conduction in CuO at room temperature.[25,49] Second is the super-superexchange J_2 which is −39 meV yet is still three times smaller than J_z. The remaining values are −17.4 meV for J_a, +3.0 meV for J_x, and +2.6 meV for J_b. From this we can directly compute E_a^{spin} according to Eq. 5.

$$E_a^{spin} = -\sum_{i<j} J_{ij}\Delta\left(\widehat{S}_i \cdot \widehat{S}_j\right). \tag{5}$$

In CuO, $-\sum_{i<j} J_{ij}\Delta\left(\widehat{S}_i \cdot \widehat{S}_j\right) = -(J_z + J_x + J_a + 2J_b + J_2)$, which gives E_a^{spin} to be 160 meV, a similar magnitude to E_a^{e-ph} (99 meV) as shown in Table 1. This result validates that E_a^{spin} contributes significantly to the overall activation energy. Therefore, this result suggests that dopants that can reduce the magnetic coupling contribution E_a^{spin}as well as the electron−phonon contribution $E_a^{e-ph}$to the activation energy can more effectively improve hole mobility in CuO.

Note that here we consider hopping along the ferromagnetic (FM) [101] direction (see Fig. 2) due to shorter Cu−Cu distances and superior orbital overlap between initial and final states. Meanwhile, we find that hopping along the antiferromagnetic (AFM) [10$\bar{1}$] direction is energetically unlikely to occur (Figure S10-S12).

Table 1. Effect of Li doping on the electron−phonon activation energy from Eq. 8

Li (%)	ε_∞	ε_0	ε_p	E_a^{e-ph} (meV)
0	6.4	11.0	15.5	99
6.25	7.9	13.0	16.7	92
12.5	8.4	16.3	17.5	88

Spin polaron conduction in Li-doped CuO from first-principles

Our experimental work (discussed later) shows Li-doped CuO electrodes have significantly increased photocurrent and show a positive shift of onset potential, while also retaining a similar crystallinity and photon absorption to the pristine CuO electrodes. Thus, it is anticipated that Li doping in CuO improves electron−hole separation and/or carrier conduction (concentration and/or mobility). To confirm this postulation, we applied our theoretical techniques discussed above to clarify how Li doping improves hole conduction in CuO.

The enhancement of carrier concentration after Li doping can be confirmed by the low hole ionization energy in Li-doped CuO, which is comparable to *kT*. Specifically, the ionization energy for a p-type dopant is defined by the difference between its charge transition level (CTL) and the valence band maximum. The CTL ($\varepsilon_{q/q'}$) is defined as the value of electron chemical potential at which the stable charge state of the defect changes from *q* to *q*′, given

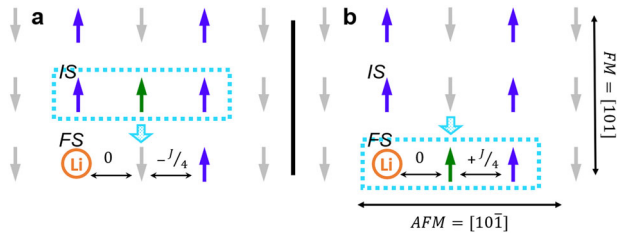

Fig. 3 Spin polaron hopping in Li-doped CuO. Diagram describing the interplay of spin and polaron hopping in CuO after Li doping (orange = Li). As the spin polaron hops through the lattice, its interaction with Li will result in a lower magnetic barrier E_a^{spin} due to broken magnetic couplings between Cu ions and nonmagnetic Li ions ($E_{spin} = 0$)

by Eq. 6.

$$\varepsilon_{q/q\prime} = \frac{E_q^f - E_{q\prime}^f}{q\prime - q} \tag{6}$$

and the formation energy E_q^f of the charge state q is defined by Eq. 7,

$$E_q^f[\varepsilon_F] = E_q - E_{prist} + \sum\nolimits_i \mu_i \Delta N_i + q\varepsilon_F, \tag{7}$$

where E_q is the total energy of the system with the charged defect, E_{prist} is the total energy of the pristine system, and the third term on the right side accounts for the change in number of atoms of each species i between these two configurations (ΔN_i), with μ_i being the atomic chemical potential of that element in its stable form. From Eqs. 6 and 7 we computed the hole ionization energy of Li-doped CuO to be 55 meV (corresponding to the −1/0 transition level). Since this energy is small and comparable to kT at room temperature, it indicates that Li introduces shallow hole states which can be ionized at room temperature to increase the hole concentration. This indicates a shift of the Fermi level towards the valence band maximum as has been experimentally shown with a positive shift of the onset potential by ~210 mV. The introduction of shallow states from Li doping is also in agreement with previous theoretical and experimental works.[28,29,50,51]

To investigate the effects of Li doping on the transport of holes in CuO (i.e. the effect of Li on hole hopping mobility) we first focused on the electron−phonon contribution to the activation energy, E_a^{e-ph}. For this part, we computed the electron−phonon activation energy of pristine and Li-doped CuO via Eq. 8. This method represents an averaged doping effect in a continuum polarization medium and avoids the sampling of all possible doping configurations and hopping paths.[52]

$$E_a^{e-ph} = \frac{e^2}{4\varepsilon_p}\left(\frac{1}{r_p} - \frac{1}{R}\right). \tag{8}$$

Here r_p is the polaron radius which is approximated as $r_p = \frac{1}{2}\left(\frac{\pi}{6}\right)^{1/3} V^{1/3}$, R is the average hopping distance, and $\frac{1}{\varepsilon_p} = \frac{1}{\varepsilon_\infty} - \frac{1}{\varepsilon_0}$ where ε_∞ is the high frequency dielectric constant and ε_0 is the static dielectric constant. The results of this calculation (Table 1) show that Li doping increased the high frequency dielectric constant (ε_∞) due to increased carrier concentrations after Li doping. Although the static dielectric constant (ε_0) is also increased due to weaker Li−O bonds (ε_0 is inversely proportional to the bonding energy squared[53]), an increased ε_∞ dominated and resulted in an overall lower barrier (E_a^{e-ph}). For example, the barrier decreases by 11 meV after 12.5% Li doping, which corresponds to 1.5 times improvement on hopping mobility based on the $\mu \propto e^{-E_a/kT}$ relation between E_a and mobility μ. Therefore, Li doping assists the electron−phonon kinetics of carriers in CuO.

To consider the effect of Li on the magnetic contribution to the activation energy E_a^{spin}, we first recalculated the magnetic couplings in CuO after a significant amount of Li doping (12.5%) using the same methods as before (Figure S8, Table S3-S4). We find that the predominate magnetic coupling J_z is nearly the same after Li doping, although overall Li suppresses the anti-ferromagnetism of CuO due to the spinless character of Li, which has also been seen experimentally.[27] The resulting energy of the spin-flip process in Li-doped CuO from Eq. 5 (assuming that there are no Li near the polarons) would be 137 meV, which is smaller than 160 meV in pristine CuO (mentioned above). We note that the largest benefit of Li doping is seen when we consider the interaction of neighboring SPs and Li. An analog of the spin-flip hopping process after Li doping in CuO is shown in Fig. 3. Since Li is nonmagnetic, it does not interact with a SP when it passes by, and a single Li site can reduce the local hopping barrier of the SP by up to 55 meV which corresponds to approximately 9 times improvement of hopping mobility based on the $\mu \propto e^{-E_a/kT}$ relation (the case of Li breaking J_z coupling). This larger effect of Li doping on the activation energy describes how Li doping significantly enhances the hole mobility in CuO, in agreement with previous experimental measurements of the activation energy of Li-doped CuO.[27,29,31,32] For example in ref. [27] a monotonic decrease of activation energy has been observed as a function of Li doping concentration (up to 16%), accompanied by strong suppression of the anti-ferromagnetism of CuO. The activation energy decreases from 0.23 eV for pristine CuO to 0.035 eV for $Cu_{0.92}Li_{0.08}O$, which leads to a three order of magnitude decrease of resistivity in experiments.[27] Since what we have discussed is relevant for isolated Li doping (Li−Li interaction is neglected in our magnetic interaction models), even a small amount of Li doping will have a significant impact on the conduction of holes in CuO and can dramatically increase the photocurrent density of CuO as we have seen in our experimental investigation.[32]

Synthesis of CuO and Li-doped CuO electrodes

CuO and Li-doped CuO electrodes were prepared to experimentally investigate the effect of Li doping and confirm the results obtained from the computational studies. In order to unambiguously identify the effect of Li doping on the charge transport properties, it is critical that other features (e.g. crystallinity and morphology) of the CuO and Li-doped CuO electrodes are the same. If a condition/procedure used for Li doping significantly alters other properties of the CuO film, any difference in properties observed between the CuO and Li-doped CuO electrodes cannot be confidently identified as the effect of Li doping.

Previously, we have demonstrated that nanofibrous CuO electrodes can be prepared by using electrodeposited $Cu_4SO_4(OH)_6$ films as precursors.[54] The electrodeposited $Cu_4SO_4(OH)_6$ films are composed of blade-like nanocrystals due to the two dimensional crystal structure of $Cu_4SO_4(OH)_6$ (Figure S14A). When immersed in 0.01 M NaOH solution (pH 12), they were converted to fibrous $Cu(OH)_2$ films (Figure S14B), which could be converted to fibrous CuO films by annealing for 3 h at 500 °C.

The same procedure could be used to produce Li-CuO by simply dropcasting a solution of $LiNO_3$ onto the $Cu(OH)_2$ films before annealing. It was expected that the nanofibrous morphology of the $Cu(OH)_2$ film can facilitate solid state diffusion of Li ions into the CuO lattice and form a uniformly Li-doped CuO film. The contents of Li in the Li-doped CuO films were determined by inductively coupled plasma mass spectrometry (ICP-MS). The scanning electron microscope (SEM) images of a pristine CuO electrode and a CuO electrode containing 0.1 at.% Li (at.% of Li = 100 × [mol of Li] / [mol of Cu + mol of Li]) are shown in Fig. 4 where no noticeable morphological differences are observed. The substitutional nature of Li doping where Li replaces Cu could be confirmed by the shifts of the Bragg peaks in the XRD patterns (Figure S15A). Although the degree of shift was very subtle, as the

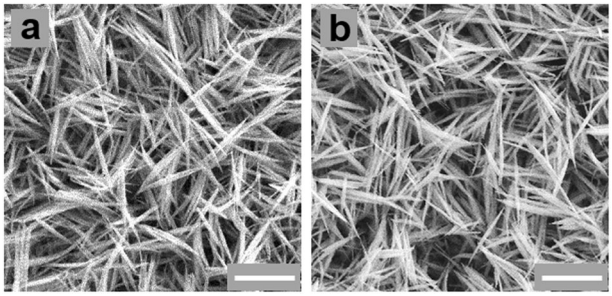

Fig. 4 SEM images of **a** CuO and **b** Li-doped CuO used in this study (the scale bar in the lower right corner designates 1 μm)

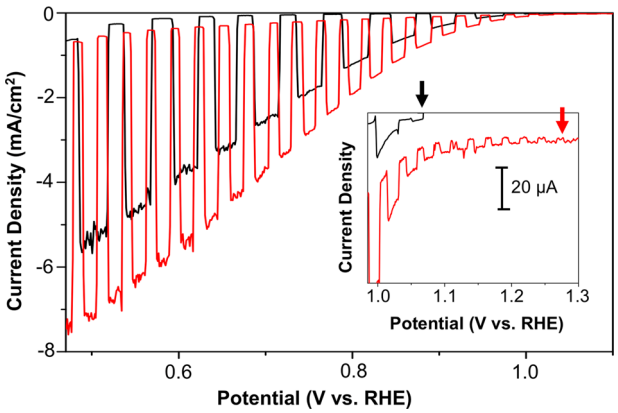

Fig. 5 $J-V$ plots (scan rate = 10 mV/s) of CuO (black) and Li-doped CuO (red) electrodes for O_2 reduction in 0.1 M KOH (pH 13) solution with O_2 purging under AM1.5G,100 mW/cm^2 illumination. The inset shows the enlarged current in the potential region near the photocurrent onset potentials indicated by arrows

doping amount is only 0.1 at. %, the peaks shifted to higher two theta values indicating a shrinking of the crystal lattice because Li^+ is smaller than Cu^{2+}. These two electrodes also showed almost identical UV−Vis absorption spectra (bandgap = 1.4 eV) (Figure S15B), indicating that Li doping does not affect photon absorption by CuO, which is consistent with our theoretical calculation of the Li-doped CuO band structure (Figure S13).

Experimental comparison of photoelectrochemical properties of CuO and Li-doped CuO electrodes

Since the direct measurement of charge transport properties of our high surface area, nanofibrous polycrystalline electrodes was not possible, the effect of Li doping on charge transport properties was evaluated by comparing photocurrent generation of CuO and Li-doped CuO electrodes. Since these electrodes have the same absorbance (Figure S15B), the number of electron−hole pairs generated in these electrodes under illumination must be identical. Then, if an interfacial charge transfer reaction that can quickly consume almost all the surface-reaching electrons is chosen for photocurrent measurement, any change in photocurrent generation caused by Li doping must be due to a change in the number of surface-reaching electrons caused by a change in the charge transport properties, which affects electron−hole separation.

For this purpose, comparing photocurrent for water reduction may not be proper because the surface of CuO is not catalytic for water reduction, and a significant portion of the surface-reaching electrons can be lost to surface recombination, making it difficult to accurately evaluate the change in the number of surface-reaching electrons. In this study, we used oxygen reduction as the photoelectrochemical reduction reaction that occurs on the CuO surface as the kinetics of this reaction is typically much faster than water reduction on oxide-based photocathodes.[54–57] The $J-V$ plots of CuO and Li-doped CuO for oxygen reduction obtained in a 0.1 M KOH (pH 13) solution purged with O_2 under standard illumination conditions (AM1.5G, 100 mW/cm^2) are shown in Fig. 5.

The pristine CuO electrode already shows efficient photocurrent generation for O_2 reduction as its bandgap allows for the utilization of a great portion of the visible solar spectrum, and its nanostructure reduces bulk electron-hole recombination. For example, it achieved a photocurrent density of ~1.2 mA/cm^2 at a potential as positive as 0.8 V vs. RHE, and it increased up to ~4.0 mA/cm^2 when the potential was swept to 0.6 V. (The dark current initiating around 0.65 V vs. RHE is due to electrochemical reduction of O_2 which was subtracted from the photocurrent to determine overall photocurrent.) The photocurrent observed for O_2 reduction can be considered the upper limit of photocurrent that can be observed for water reduction when an efficient hydrogen evolution catalyst is placed on the CuO surface to improve the water reduction kinetics.

The Li-doped CuO electrode significantly enhanced photocurrent generation. For example, the Li-doped CuO electrode achieved a photocurrent density of ~2.0 mA/cm^2 at a potential as positive as 0.8 V vs. RHE, and it increased up to ~5.6 mA/cm^2 when the potential was swept to 0.6 V. In addition to the evident increase in magnitude of photocurrent density, Li-doped CuO electrodes demonstrated a considerable shift in photocurrent onset to the positive direction by ~210 mV. The photocurrent onset potential for a reaction that has high interfacial charge transfer kinetics, such as O_2 reduction on an oxide photocathode, can be considered the flatband potential. This is because for such reactions the loss of the surface-reaching minority carriers to surface recombination is negligible. In this case, it can be assumed that photocurrent disappears when the applied potential is the same as the flatband potential, where electron−hole separation is no longer possible. The fact that the $J-V$ plots of CuO and Li-doped CuO electrodes measured with chopped illumination do not show any transient photocurrent even when the applied potential is near the photocurrent onset potential is a good indication that recombination on the CuO surface during O_2 reduction is negligible. This confirms that the photocurrent onset potentials of these electrodes can be regarded as their flatband potentials. Since the flatband potential is the same as the Fermi level after accounting for the Helmholtz layer potential drop at the semiconductor/electrolyte interface, and the Helmholtz layer potential drop should not be altered by 0.1 at.% Li doping, the shift of the onset potential of Li-doped CuO directly indicates that Li doping shifted the Fermi level of CuO to the positive direction, closer to the valance band maximum.[58]

These experimentally obtained results agree well with the computational results that Li doping generates shallow acceptors that effectively increase the hole concentration. The increase in hole concentration, which improves the hole conductivity, can reduce electron−hole recombination in the bulk or in the space charge region, increasing the number of minority carriers reaching the surface to perform oxygen reduction. Also, the increase in hole density that changed the Fermi level was confirmed by the shift of the flatband potential to the positive direction. Finally, according to our computational results, a simultaneous decrease in E_a by Li doping also contributed to photocurrent enhancement by improving the hole mobility of CuO.

While the impact of Li doping on the activation energy E_a and on carrier density cannot be easily separated in our photocurrent measurements, the impact of Li doping on the activation energy has been discussed explicitly in dark resistivity measurements of Li-doped CuO between a few K to 300 K.[27,29] An order of magnitude decrease of the hopping activation energy with 16 at.% Li doping clearly confirmed the combined effect of E_a^{spin} and

E_a^{e-ph} being lowered by Li doping, as the effect of E_a^{e-ph} alone cannot explain the observed order of magnitude decrease in the hopping activation energy based on our calculations.[27] This study clearly demonstrated that the effect of Li doping on E_a^{spin} is still considerable at 300 K (because of the short-range magnetic couplings remaining above Néel temperature)[25,49] and that Li doping can play a critical role in improving the mobility of CuO at room temperature, which is relevant for its PEC applications.

In conclusion, we have studied in-depth hole conduction in pristine and Li-doped CuO by first-principles calculations accompanied by the PEC performance of experimentally prepared CuO and Li-doped CuO electrodes. In pristine CuO, we have verified the existence of spin polarons (SP), which occur via the flip of a single Cu ion's spin so that the polaron may redistribute over several atoms, and this delocalization effect lowers the energy of the polaron state. We then showed how transport of SPs in CuO will involve a spin-flip hopping process and developed a theoretical framework of computing the activation energy which involves both electron−phonon and magnetic coupling contributions. Next, we displayed how Li doping in CuO generates shallow states above the valence band which pushes the Fermi level closer to the valence band maximum and improves hole concentrations in CuO. Then, we showed how Li doping improves hole hopping mobility in CuO by lowering the electron−phonon coupling contribution to the activation energy due to higher electronic screening. More importantly, we demonstrated that Li doping lowers the magnetic coupling contribution to the activation energy due to the destruction of magnetic interactions through the replacement of Cu ions with nonmagnetic Li ions, culminating in a significantly lowered hopping barrier and increased hole mobility in Li-doped CuO. Finally, we prepared CuO and Li-doped CuO electrodes and compared their photoelectrochemical properties for O_2 reduction, where the changes in photocurrent and the onset of photocurrent can be directly related to changes in charge transport properties and the Fermi level, respectively. The experimental results show that Li doping enhances charge transport properties and shifted the Fermi level toward the valence band maximum while not affecting photon absorption, which agrees well with the computational results. This work provides important insights on the mechanisms of the formation and transport of SPs and their effect on the charge transport properties of CuO and Li-doped CuO. Similar to Li doping, doping with other nonmagnetic shallow acceptors may also simultaneously improve carrier concentration and hopping mobility of magnetic oxides. In this case, shallow dopants can be ionized easily to increase carrier concentrations and increase dielectric screening, which weakens the charge−lattice interactions. Most importantly, nonmagnetic dopants can break the magnetic couplings and lower the hopping barrier for SPs significantly, which is critical for improvement of hopping mobility. These insights offer effective strategies for the improvement of hopping conduction in magnetic oxides through atomic doping, which provides important guidance for materials design.

METHODS

Cupric oxide (CuO) assembles in a monoclinic structure with C2/c symmetry and a geometric unit cell consisting of only eight atoms. To consider the correct magnetic interactions prevalent in CuO, a $\sqrt{2}\times 1\times \sqrt{2}$ unit cell containing 16 atoms needs to be implemented (Figure S1).[47,49,59] Meanwhile, a $2\times 3\times 2$ supercell of 96 atoms was used for calculations considering polaron formation and doping. A final supercell of $2\sqrt{2}\times 3\times 2\sqrt{2}$ with 192 atoms was used to confirm spin polaron formation size and charged cell correction.

It is well known that both local and semi-local exchange and correlation functionals in DFT cannot accurately describe the electron correlation in magnetic insulators, which results in a qualitatively incorrect electronic structure. To account for this issue, we applied the Hubbard U correction[60] with $U = 7.5$ eV, a well-established model for this material.[50,51,61–63] All calculations were carried out in the open-source plane wave code Quantum ESPRESSO[64] with ultrasoft LDA pseudopotentials,[65] unless otherwise noted. The choice of LSDA+U instead of GGA+U was made because GGA+U was unable to give the correct monoclinic structure of CuO, while LSDA+U yielded a geometry of CuO within 5% of experimental values. Nonetheless, LSDA+U and GGA+U provide similar electronic structures (with the experimental geometry) and overall gave results in agreement with the experimental expectations. Our calculations yielded that Cu^{2+} ions have a magnetic moment of 0.57 μ_B with a magnetic ordering according to Figure S1. Notably, the O atoms in this system share a non-negligible magnetic moment of 0.14 μ_B (in agreement with previous experiments[59] and theory[50]). We were also able to replicate the computed magnetic couplings at higher levels of theory with the LSDA+U method (see Table S1-S2). We have noted that one previous study also considered applying a Hubbard correction on O p state.[66] While this current study does not employ a Hubbard U on O p states, we found that spin polaron characteristics relevant to our study do not change upon applying a U on O p (Figure S5-S6), and the conclusions in this work are unaffected by the choice of U on O p.

DATA AVAILABILITY

The data that support the findings of this study and the code for the first-principles methods proposed in this study are available from the corresponding authors (Yuan Ping and Kyoung-Shin Choi) upon reasonable request.

ACKNOWLEDGEMENTS

Y.P. acknowledges financial support from the National Science Foundation under grant no. DMR-1760260 and the Hellman Fellowship. T.J.S. acknowledges financial support from a GAANN fellowship. This research used resources of the Center for Functional Nanomaterials, which is a U.S. DOE Office of Science Facility, and the Scientific Data and Computing Center, a component of the Computational Science Initiative, at Brookhaven National Laboratory under Contract No. DE-SC0012704. This work also used the Extreme Science and Engineering Discovery Environment (XSEDE),[67] which is supported by National Science Foundation grant number ACI-1548562. K.-S.C. acknowledges financial support from the Division of Chemical Sciences, Geosciences, and Biosciences, Office of Basic Energy Sciences of the U.S. Department of Energy through Grant DE-SC0008707. A.C.C. was supported by the National Science Foundation Graduate Research Fellowship under Grant No. DGE-1256259.

AUTHOR CONTRIBUTIONS

Y.P. established the theoretical models and supervised the theoretical part of the project, T.J.S. and F.W. performed the calculations and data analysis, K.-S.C. designed the experiments and supervised the experimental part of the project, A.C.C. performed the experiments, Y.P. and K.-S.C. discussed the results, and all authors participated in the writing of the paper.

ADDITIONAL INFORMATION

Supplementary information accompanies the paper on the *npj Computational Materials* website (https://doi.org/10.1038/s41524-018-0118-3).

Competing interests: The authors declare no competing interests.

Publisher's note: Springer Nature remains neutral with regard to jurisdictional claims in published maps and institutional affiliations.

REFERENCES

1. Abdi, F. F. & Berglund, S. P. Recent developments in complex metal oxide photoelectrodes. *J. Phys. D Appl. Phys.* **50**, 193002 (2017).
2. Rettie, A. J. E., Chemelewski, W. D., Emin, D. & Mullins, C. B. Unravelling small-polaron transport in metal oxide photoelectrodes. *J. Phys. Chem. Lett.* **7**, 471–479 (2016).
3. Smart, T. J. & Ping, Y. Effect of defects on the small polaron formation and transport properties of hematite from first-principles calculations. *J. Phys. Condens. Matter* **29**, 394006 (2017).

4. Kim, T. W., Ping, Y., Galli, G. A. & Choi, K. S. Simultaneous enhancements in photon absorption and charge transport of bismuth vanadate photoanodes for solar water splitting. *Nat. Commun.* **6**, 87689 (2015).
5. Jang, Y. J. et al. Tree branch-shaped cupric oxide for highly effective photoelectrochemical water reduction. *Nanoscale* **7**, 7624–7631 (2015).
6. Koffyberg, F. P. & Benko, F. A. A photo-electrochemical determination of the position of the conduction and valence band edges of p-type CuO. *J. Appl. Phys.* **53**, 1173–1177 (1982).
7. Chiang, C. Y., Shin, Y., Aroh, K. & Ehrman, S. Copper oxide photocathodes prepared by a solution based process. *Int. J. Hydrog. Energ.* **37**, 8232–8239 (2012).
8. Izaki, M. et al. Electrodeposition of 1.4-eV-bandgap p-copper (II) oxide film with excellent photoactivity. *J. Electrochem. Soc.* **158**, D578–D584 (2011).
9. Sagu, J. S., Peiris, T. A. N. & Wijayantha, K. G. U. Rapid and simple potentiostatic deposition of copper (II) oxide thin films. *Electrochem. Commun.* **42**, 68–71 (2014).
10. Masudy-Panah, S. et al. Nanocrystal engineering of sputter-grown CuO photocathode for visible-light-driven electrochemical water splitting. *ACS Appl. Mater. Inter.* **8**, 1206–1213 (2016).
11. Lee, J. G. et al. Scalable binder-free supersonic cold spraying of nanotextured cupric oxide (CuO) films as efficient photocathodes. *ACS Appl. Mater. Inter.* **8**, 15406–15414 (2016).
12. Guo, X. et al. CuO/Pd composite photocathodes for photoelectrochemical hydrogen evolution reaction. *Int. J. Hydrog. Energ.* **39**, 7686–7696 (2014).
13. Emin, S. et al. A novel approach for the preparation of textured CuO thin films from electrodeposited CuCl and CuBr. *J. Electroanal. Chem.* **717**, 243–249 (2014).
14. Septina, W., Prabhakar, R. R., Wick, R., Moehl, T. & Tilley, S. D. Stabilized solar hydrogen production with CuO/CdS heterojunction thin film photocathodes. *Chem. Mater.* **29**, 1735–1743 (2017).
15. Wong, T. K. S., Zhuk, S., Masudy-Panah, S. & Dalapati, G. K. Current status and future prospects of copper oxide heterojunction solar cells. *Materials* **9**, 271 (2016).
16. Masudy-Panah, S. et al. Titanium doped cupric oxide for photovoltaic application. *Sol. Energ. Mat. Sol. C* **140**, 266–274 (2015).
17. Poloju, M., Jayababu, N. & Reddy, M. V. R. Improved gas sensing performance of Al doped ZnO/CuO nanocomposite based ammonia gas sensor. *Mater. Sci. Eng. B-Adv.* **227**, 61–67 (2018).
18. Rydosz, A., Maziarz, W., Pisarkiewicz, T., Wincza, K. & Gruszczynski, S. Nano-thin CuO films doped with Au and Pd for gas sensors applications. In *2013 International Conference on Informatics, Electronics & Vision (Iciev)*, Dhaka, Bangladesh (2013).
19. Rettie, A. J. E. et al. Combined charge carrier transport and photoelectrochemical characterization of BiVO4 single crystals: intrinsic behavior of a complex metal oxide. *J. Am. Chem. Soc.* **135**, 11389–11396 (2013).
20. Carneiro, L. M. et al. Excitation-wavelength-dependent small polaron trapping of photoexcited carriers in alpha-Fe2O3. *Nat. Mater.* **16**, 819–825 (2017).
21. Devreese, J. T. In George L. Trigg (Ed.). *Encyclopedia of Applied Physics* Vol. 14, 383 (VCH Publishers, New York, 1996).
22. Mott, N. F. Conduction in glasses containing transition metal ions. *J. Non-Cryst. Solids* **1**, 1–17 (1968).
23. Samokhvalov, A. A. et al. Small mobile charge-carriers in CuO. *Zh. Eksp. Teor.* **103**, 951–961 (1993). *Fiz+*.
24. Wu, J. N., Yin, B., Wu, F., Myung, Y. & Banerjee, P. Charge transport in single CuO nanowires. *Appl. Phys. Lett.* **105**, 183506 (2014).
25. Zheng, X. G. et al. Evidence of charge stripes, charge-spin-orbital coupling and phase transition in a simple copper oxide CuO. *J. Phys. Soc. Jpn.* **70**, 1054–1063 (2001).
26. Jeong, Y. K. & Choi, G. M. Nonstoichiometry and electrical conduction of CuO. *J. Phys. Chem. Solids* **57**, 81–84 (1996).
27. Zheng, X. G. et al. Fast suppression of antiferromagnetism in Cu1-xLixO. *Phy. Rev. B* **69**, 094510 (2004).
28. Choi, Y. H., Kim, D. H. & Hong, S. H. p-Type aliovalent Li(I) or Fe(III)-doped CuO hollow spheres self-organized by cationic complex ink printing: structural and gas sensing characteristics. *Sens. Actuat. B-Chem.* **243**, 262–270 (2017).
29. Gao, K. H., Li, Z. Q., Du, T., Jiang, E. Y. & Li, Y. X. Ferromagnetic properties of bulk Cu1-xMnxO magnetic semiconductors. *Phys. Rev. B* **75**, 174444 (2007).
30. Masudy-Panah, S. et al. Optical bandgap widening and phase transformation of nitrogen doped cupric oxide. *J. Appl. Phys.* **118**, 225301 (2015).
31. Zheng, X. G., Yamada, H., Scanderbeg, D. J., Maple, M. B. & Xu, C. N. Effect of hole doping in LixCu1-xO. *Phys. Rev. B* **67**, 214516 (2003).
32. Chiang, C. Y., Shin, Y. & Ehrman, S. Dopant effects on conductivity in copper oxide photoelectrochemical cells. *Appl. Energ.* **164**, 1039–1042 (2016).
33. Chiang, C. Y., Shin, Y. & Ehrman, S. Li doped CuO film electrodes for photoelectrochemical cells. *J. Electrochem. Soc.* **159**, B227–B231 (2012).
34. Chand, P., Gaur, A., Kumar, A. & Gaur, U. K. Structural and optical study of Li doped CuO thin films on Si (1 0 0) substrate deposited by pulsed laser deposition. *Appl. Surf. Sci.* **307**, 280–286 (2014).
35. Ghijsen, J. et al. Electronic-structure of Cu_2O and CuO. *Phys. Rev. B* **38**, 11322–11330 (1988).
36. De Gennes, P. Interactions indirectes entre couches 4f dans les métaux de terres rares. *J. Phys.-Paris* **23**, 510–521 (1962).
37. Vigren, D. T. Mobility of self-trapped paramagnetic spin polaron. *J. Phys. C. Solid State* **6**, 967–975 (1973).
38. Mott, N. F. Polaron models of high-temparature superconductors. *J. Phys. Condens. Matter* **5**, 3487–3506 (1993).
39. Chernyshev, A. L. & Wood, R. F. Spin polarons and high-T(c) superconductivity. In J. K. Srivastava, S. M. Rao (Ed.). *Models and Methods of High-Tc Superconductivity Some Frontal Aspects* Vol. 2, 339–382 (Nova Science Publishers, New York, 2003).
40. Lu, J. P. & Si, Q. M. Spin polarons in high-Tc copper oxides: differences between electron-doped and hole-doped systems. *Phys. Rev. B* **42**, 950–953 (1990).
41. Yonemitsu, K., Bishop, A. R. & Lorenzana, J. Sensitivity of doping states in the copper oxides to electron-lattice coupling. *Phys. Rev. Lett.* **69**, 965–968 (1992).
42. Alexandrov, A. S. & Mott, N. F. Bipolarons. *Rep. Prog. Phys.* **57**, 1197–1288 (1994).
43. Wood, R. F. & Cooke, J. F. d9 spin-polaron theory of high-Tc superconductivity. *Phys. Rev. B* **45**, 5585–5606 (1992).
44. Goldey, M. B., Brawand, N. P., Voros, M. & Galli, G. Charge transport in nanostructured materials: implementation and verification of constrained density functional theory. *J. Chem. Theory Comput.* **13**, 2581–2590 (2017).
45. Kaduk, B., Kowalczyk, T. & Van Voorhis, T. Constrained density functional theory. *Chem. Rev.* **112**, 321–370 (2012).
46. Rocquefelte, X. et al. Short-range magnetic order and temperature-dependent properties of cupric oxide. *J. Phys. Condens. Matter* **22**, 045502 (2010).
47. Rocquefelte, X., Schwarz, K. & Blaha, P. Theoretical investigation of the magnetic exchange interactions in copper(II) oxides under chemical and physical pressures. *Sci. Rep.* **2**, 759 (2012).
48. Rocquefelte, X., Schwarz, K., Blaha, P., Kumar, S. & van den Brink, J. Room-temperature spin-spiral multiferroicity in high-pressure cupric oxide. *Nat. Commun.* **4**, 2511 (2013).
49. Yang, B. X., Thurston, T. R., Tranquada, J. M. & Shirane, G. Magnetic neutron-scattering study of single-crystal cupric oxide. *Phys. Rev. B* **39**, 4343–4349 (1989).
50. Peng, Y. et al. Density functional theory analysis of dopants in cupric oxide. *J. Appl. Phys.* **111**, 103708 (2012).
51. Peng, Y., Zheng, J. W., Wu, P. & Wang, J. L. Ab-initio study of donor-acceptor codoping for n-type CuO. *J. Appl. Phys.* **116**, 163704 (2014).
52. Austin, I. G. & Mott, N. F. Polarons in crystalline and non-crystalline materials. *Adv. Phys.* **18**, 41–102 (1969).
53. Gonze, X. & Lee, C. Dynamical matrices, born effective charges, dielectric permittivity tensors, and interatomic force constants from density-functional perturbation theory. *Phys. Rev. B* **55**, 10355–10368 (1997).
54. Cardiel, A. C., McDonald, K. J. & Choi, K.-S. Electrochemical growth of copper hydroxy double salt films and their conversion to nanostructured p-type CuO photocathodes. *Langmuir* **33**, 9262–9270 (2017).
55. Kang, D., Hill, J. C., Park, Y. & Choi, K.-S. Photoelectrochemical properties and photostabilities of high surface area CuBi2O4 and Ag-doped CuBi2O4 photocathodes. *Chem. Mater.* **28**, 4331–4340 (2016).
56. Read, C. G., Park, Y. & Choi, K.-S. Electrochemical synthesis of p-type CuFeO2 electrodes for use in a photoelectrochemical cell. *J. Phys. Chem. Lett.* **3**, 1872–1876 (2012).
57. Wheeler, G. P. & Choi, K.-S. Photoelectrochemical properties and stability of nanoporous p-type LaFeO3 photoelectrodes prepared by electrodeposition. *ACS Energy Lett.* **2**, 2378–2382 (2017).
58. Nozik, A. J. Photoelectrochemistry: applications to solar energy conversion. *Annu. Rev. Phys. Chem.* **29**, 189–222 (1978).
59. Forsyth, J. B., Brown, P. J. & Wanklyn, B. M. Magnetism in cupric oxide. *J. Phys. C Solid State* **21**, 2917–2929 (1988).
60. Dudarev, S. L., Botton, G. A., Savrasov, S. Y., Humphreys, C. J. & Sutton, A. P. Electron-energy-loss spectra and the structural stability of nickel oxide: An LSDA + U study. *Phys. Rev. B* **57**, 1505–1509 (1998).
61. Heinemann, M., Eifert, B. & Heiliger, C. Band structure and phase stability of the copper oxides Cu2O, CuO, and Cu4O3. *Phys. Rev. B* **87**, 115111 (2013).
62. Debbichi, L., de Lucas, M. C. M., Pierson, J. F. & Kruger, P. Vibrational properties of CuO and Cu4O3 from first-principles calculations, and raman and infrared spectroscopy. *J. Phys. Chem. C* **116**, 10232–10237 (2012).
63. Wu, D. X., Zhang, Q. M. & Tao, M. LSDA+U study of cupric oxide: electronic structure and native point defects. *Phys. Rev. B* **73**, 235206 (2006).
64. Giannozzi, P. et al. Quantum ESPRESSO: a modular and open-source software project for quantum simulations of materials. *J. Phys. Condens. Matter* **21**, 395502 (2009).
65. Garrity, K. F., Bennett, J. W., Rabe, K. M. & Vanderbilt, D. Pseudopotentials for high-throughput DFT calculations. *Comp. Mater. Sci.* **81**, 446–452 (2014).
66. Himmetoglu, B., Wentzcovitch, R. M. & Cococcioni, M. First-principles study of electronic and structural properties of CuO. *Phys. Rev. B* **84**, 115108 (2011).

67. Towns, J. et al. XSEDE: accelerating scientific discovery. *Comput. Sci. Eng.* **16**, 62–74 (2014).